Nonlocal Kardar-Parisi-Zhang equation to model interface growth

Persefoni Kechagia and Yanis C. Yortsos
Department of Chemical Engineering, University of Southern California, Los Angeles, California 90089-1211

Peter Lichtner
Division of Earth and Environmental Sciences, Los Alamos National Laboratory, Los Alamos, New Mexico 87545

(Received 3 August 2000; revised manuscript received 16 January 2001; published 26 June 2001)

The dynamics of the growth of interfaces in the presence of noise and when the normal velocity is constant, in the weakly nonlinear limit, are described by the Kardar-Parisi-Zhang (KPZ) equation. In many applications, however, the growth is controlled by nonlocal transport, which is not contained in the original KPZ equation. For these problems we are proposing an extension of the KPZ model, where the nonlocal contribution is expressed through a Hilbert transform and can act to either stabilize or destabilize the interface. The model is illustrated with a specific example from reactive infiltration. The properties of the solution of the resulting equation are studied in one spatial dimension in the linear and the nonlinear limits, for both stable and unstable growth. We find that the early-time behavior has a power-law scaling similar to that of the KPZ equation. However, in the case of stable growth, the scaling of the saturation width is logarithmic, which differs from the power law in the KPZ equation. This dependence reflects the stabilizing effect of nonlocal transport. In the unstable case, we obtain results similar to those of Olami *et al.* [Phys. Rev. E **55**, 2649 (1997)].

DOI: 10.1103/PhysRevE.64.016315 PACS number(s): 47.27.Jv, 47.55.Mh, 47.70.Fw, 05.45.−a

I. INTRODUCTION

The evolution of interfaces growing in a direction normal to themselves, in the presence of noise and interfacial smoothing, was described in a pioneering paper by Kardar, Parisi, and Zhang [1]. These authors proposed a Langevin-type equation

$$\frac{\partial h}{\partial t} = \nu \nabla^2 h + \frac{\lambda}{2}(\nabla h)^2 + \eta(\mathbf{x},t) \tag{1}$$

commonly known as the KPZ-equation, for the evolution of the fluctuation $h(\mathbf{x},t)$ of the height of the interface from its mean. In this equation, the first term on the right-hand side describes interfacial smoothing by a surface tension ν in a direction lateral to the main growth, and the second is the leading-order term for growth in a direction normal to the interface, where λ is the growth velocity. The noise $\eta(\mathbf{x},t)$ is an uncorrelated Gaussian with zero mean and amplitude D, satisfying $\langle \eta(\mathbf{x},t)\rangle = 0$ and $\langle \eta(\mathbf{x},t)\,\eta(\mathbf{x}',t')\rangle = 2D\delta^d(\mathbf{x}-\mathbf{x}')\,\delta(t-t')$, where d is the dimension of the interface and δ^d is the d-dimensional delta function.

The properties of the KPZ equation have been studied in great detail. Its considerable interest stems from the fact that Eq. (1) is prototypical of self-affine growth with exponents that are universal (for example, see [2] and references therein). Methods such as the dynamic renormalization group [1] have been used to obtain insight into its scaling properties and exponents. Equation (1) is also the weakly nonlinear expansion in the presence of noise of a linear equation with the spectral relationship

$$\omega = -\nu \mathbf{k}^2, \tag{2}$$

where ω is the rate of growth corresponding to wave number $\mathbf{k}$ [and where we have assumed $h \sim \exp(\omega t + i\mathbf{k}\cdot\mathbf{x})$]. Dispersion relation (2) shows that the process described by the KPZ equation is linearly stable ($\omega < 0$) for all $\mathbf{k}$.

The KPZ equation and its variants have been used to describe a variety of processes, from ballistic deposition [3] to the formation of cell colonies in bacteria or tissue cultures (Eden model) [4,5], randomly stirred fluids [6], and directed polymers in random media [7]. Of interest to this work, however, has been a more recent observation by Aharonov and Rothman [8], who suggested that the KPZ equation can also describe the evolution of the pore-grain interface in sedimentary rocks when the process is reaction controlled. In the particular approach in [8] the relative height (asperity) h of the grain surface grows due to a chemical reaction involving the pore fluid. The process is kinetically controlled, and the growth is at a constant velocity, determined from the reaction kinetics. We define $f(z,t,x) = z - F(t,x) = 0$. For example, if the reaction occurs everywhere at the constant rate λ, then the normal velocity v_n of the front $z = F(t,\mathbf{x})$, in the absence of interfacial smoothing and noise, would be constant,

$$v_n \equiv \frac{-F_t}{|\nabla F|} = \lambda. \tag{3}$$

For a KPZ-like equation, one takes the weakly nonlinear limit, in which case Eq. (3) leads to

$$F_t = \lambda\left(1 + \tfrac{1}{2}|\nabla F|^2 + \cdots\right). \tag{4}$$

By defining the relative height $h = F - \lambda t$, one then obtains

$$h_t = \frac{\lambda}{2}|\nabla h|^2 + \cdots, \tag{5}$$

which constitutes the nonlinear part of the KPZ equation. Addition of a diffusion term and noise then leads to the KPZ equation.

In many processes involving reaction-induced morphology changes in porous media, however, reaction rates are not necessarily slow, while the growth process may be controlled by (nonlocal) transport, for example, by diffusion or convection. Indeed, this would also be the case for the process in [8], in which diffusion toward the interface constitutes the nonlocal transport. We cite other examples from dissolution or precipitation processes [9], gas-solid reactions [10], and a variety of reaction engineering processes [11]. Here, diffusive or convective transport operates in the bulk of the fluid or of the porous medium and toward the grain interface, rather than only along the interface, as in the interfacial process envisioned in [8]. Two other examples obeying similar dynamics, but in a slightly different context, involve the displacement of one fluid by another of different viscosity in a random porous medium [12] and the propagation of laminar flames [13,14]. In these cases, the pressure fields governing fluid flow obey the Laplace equation (due to Darcy's law in the first case and to Euler's equations in the second), as in the case of steady-state diffusion, giving rise to a nonlocal term. Finally, a similar situation occurs in the acidization of a porous matrix [9,15], and more generally in reactive infiltration in porous media, an example of which will be analyzed in detail below. Changes in the mobility of the flowing phases, the expansion of fluids at the flame fronts, and the pore structure of the matrix (permeability), in the respective cases, affect the transport toward the front and in turn its evolution. These changes may result in stable or unstable fronts. Under these circumstances, the KPZ equation cannot capture the growth and coarsening dynamics, which now become nonlocal.

To account for problems in which nonlocal transport is dominant and cannot be neglected, we propose in this paper an extension of the KPZ equation, by adding to Eq. (1) a term of the form $\mathcal{H}(h_x)$, where $\mathcal{H}$ is the Hilbert transform, to obtain, in the case of $1+1$ dimensions, the equation

$$h_t = \nu h_{xx} - m\mathcal{H}(h_x) + \frac{\lambda}{2}(h_x)^2 + \eta(\mathbf{x},t). \tag{6}$$

For simplicity, we will refer to Eq. (6) as the HKPZ (Hilbert-KPZ) equation. In the various applications mentioned, this modification accounts for nonlocal transport in the weakly nonlinear limits, as will be shown below. Recall that the Hilbert transform is defined as the principal value of the following integral [16]:

$$\mathcal{H}(f) = \frac{1}{\pi}\mathcal{P}\int_{-\infty}^{\infty} \frac{f(t)}{x-t}dt, \tag{7}$$

and also satisfies the following property:

$$\hat{\mathcal{H}}(h_x) = -|k|\hat{h}, \tag{8}$$

where the caret denotes the Fourier transform. We note that the somewhat similar equation

$$v_t = \nu v_{xx} - \mathcal{H}(v_x) + v v_x + \eta(\mathbf{x},t) \tag{9}$$

was proposed by Olami *et al.* [17] to investigate the propagation of combustion fronts in the presence of noise. This equation was obtained from a normalized version of Sivashinsky's equation [13], which is Eq. (6) without noise and with $\lambda = -1$, by differentiating with respect to x and subsequently adding noise. Thus, in [17] the noise is added to the growth of the slope of the front, rather than to the growth of the front itself, contrary to the case in the HKPZ (and the KPZ) equation. Note also that Eq. (9) corresponds to unstable growth ($m = 1 > 0$).

In this paper we will study the properties of the general equation (6) by proceeding as follow. We provide a derivation of the HKPZ equation, first by using general physical arguments and subsequently by focusing on the specific problem of reactive infiltration under fast kinetics. Its solution in one space dimension is considered next. We develop a numerical scheme using finite differences and a fast Fourier transform, which is tested against available analytical results in the absence of noise. Then the linearized version of the HKPZ equation, which is the counterpart of the Edwards-Wilkinson (EW) equation [18], is analyzed. We develop asymptotics for early and late times, which allow for the roughness exponents (if any) of the linearized HKPZ equation to be derived. Results are presented for both the stable and unstable cases. Then the full HKPZ equation is solved numerically in one spatial dimension. The scaling behavior of the results is investigated in the small and large time limits.

II. DERIVATION OF THE HKPZ EQUATION

In this section we provide a derivation of the HKPZ equation, first by using general arguments and subsequently by considering a specific example from reactive infiltration in a porous medium. We also discuss briefly the process envisioned in [8] and show that it must also belong to the general problem described by the HKPZ equation.

In general, deriving a HKPZ equation corresponding to the processes described above consists of the following steps: defining a base state corresponding to a planar interface, conducting a linear stability analysis, deriving the linear dispersion relation, which must correspond to the linearized HKPZ equation, considering a long-wave expansion near the onset of the nonlocal behavior, taking the weakly nonlinear limit, and adding noise. For example, all but the last steps were taken by Sivashinsky [13] in his analysis of the long-wave hydrodynamic stability of flames. Olami *et al.* [17] added noise as explained above and studied the evolution of unstable fronts.

As noted previously, for the result to be of the HKPZ type, the linear dispersion relation must include a nonlocal term of the form

$$\omega = m|k| - \nu k^2 + \cdots \tag{10}$$

[e.g., compare to Eq. (2)]. Then the linear process is unconditionally stable if $m<0$ and conditionally unstable if $m>0$. The term involving $|k|$ reflects nonlocal transport, arising from the solution of a Laplace equation at long wavelengths, and corresponds in the HKPZ equation to the Hilbert

transform. The fact that the latter represents the flux at the interface at $y=0$ arising from the solution of the Laplace equation, can be seen simply by writing a conservation equation of the type

$$h_t - m h_y = \nu h_{xx} \quad \text{at } y=0 \tag{11}$$

and by extending the function h to be a harmonic function in the upper half plane ($y>0$), namely, by taking

$$h_{xx} + h_{yy} = 0 \quad \text{for } y>0. \tag{12}$$

Then, if we introduce the analytic function $w=h+i\mathcal{H}(h)$, use of the Cauchy-Riemann conditions shows that $h_y|_{y=0} = -\mathcal{H}(h_x)$, as postulated. In such an interpretation, for example, of the process of [8], the flux $-\mathcal{H}(h_x)$, arriving at $y=0$, is used partly for the growth of the interface and partly to satisfy the lateral diffusion along the interface [compare with Eq. (11) and also see below]. The Laplace equation (12) may describe transport either by diffusion or by advection, when the latter is controlled by potential flow, as, for example, in the case of flow in porous media. A more rigorous derivation for the case of reactive infiltration will be described below. For future reference, we also note that in one dimension (1D) and for $m>0$ there exists a cutoff mode $k_c = m/\nu$, and a fastest growing mode $k_{\max}=m/2\nu$, with growth rate $\omega_{\max}=m^2/4\nu$.

We must note that not all processes whose linear spectral relationship is (10) lead to the HKPZ equation. The converse is true, however. In addition, if the linear limit is Eq. (10), then the nonlinear version of the process evidently cannot be of the KPZ type. Specifically, we will show below that such is the case with the model considered in [8].

The parameter m expresses a contrast in transport properties across the growing interface, with stable or unstable displacement corresponding to negative or positive m, respectively. As discussed above, long-wave dispersion relations of the type (10) arise in a variety of problems. In displacements in porous media, m is a normalized viscosity difference upstream (subscript 1) and downstream (subscript 0) of the front, $m=(\mu_0-\mu_1)/(\mu_0+\mu_1)$, as pointed out by Saffman and Taylor in Hele-Shaw flows [19] or by Yortsos and Hickernell [20] in general displacements in porous media. When the pore structure changes as a result of flow and reaction, for example, in acidization, then $m=(K_1-K_0)/(K_1+K_0)$, where K is the flow permeability [21,22]. In such applications, nonlocal growth is driven by advection which is controlled by Darcy's law. In the case of flame propagation, Sivashinsky showed that $m=(1-\sigma)$, where σ is the coefficient of thermal expansion [13]. Here, the nonlocal transport results from Euler's equations, which also give rise to potential flow. In interfacial growth problems, such as in [8], nonlocal transport is due to diffusion in the bulk. That transport problem is similar to directional solidification [23,24], where $m\sim v$ and v is the undisturbed interface velocity. The latter is positive in the case of solidification or in the case of deposition/precipitation, hence indicating instability, but negative in the case of melting or in the case of dissolution, indicating stability.

The stabilizing coefficient $\nu>0$ reflects an effective interfacial tension. In displacements in porous media it expresses capillarity, in reactive infiltration it expresses diffusion in the bulk (see below), in flame propagation it is related to the Lewis number of the component limiting the reaction, and in the process analyzed in [8] it describes interfacial diffusion along the interface. Interestingly, in the last process, diffusion acts in two different ways: in the bulk, in order to supply the necessary flux to the interface (and to destabilize or stabilize the interface depending on whether or not the interface grows or recedes, respectively) and along the interface, in order to stabilize the latter. We must point out that in problems such as solidification [23,24], where the relaxation of the interface is controlled by the Gibbs-Thomson condition, or in Hele-Shaw cell displacements [12], where the interfacial tension acts in proportion to the effective curvature of the interface, the resulting stabilization enters at order $|k|^3$. Therefore, such problems do not have the linear dispersion relation (10) and will not lead to a HKPZ equation. The ellipsis in Eq. (10) reflects the existence of additional terms in the general problem (for example, in displacements in porous media, in flame propagation, etc.) that are of higher order and do not contribute in the long-wave limit.

Taking the weakly nonlinear limit has been done in the context of flame propagation. Specifically, Sivashinsky [13] obtained the following weakly nonlinear equation:

$$h_t + \epsilon\nabla^2 h + \frac{1}{2}(\nabla h)^2 = \frac{(1-\sigma)}{8\pi^2}\int_{-\infty}^{\infty} |\mathbf{k}|\hat{h}(t,\mathbf{k}) e^{i\mathbf{k}\cdot(\mathbf{x}-\mathbf{z})} d\mathbf{k}\, d\mathbf{z} \tag{13}$$

valid at large wavelengths (in this notation $\epsilon<0$). For $1-\sigma>0$, Eq. (13) describes long-wave instability. Including only the nonlinear part, namely, by taking

$$h_t + \tfrac{1}{2}|\nabla h|^2 = 0, \tag{14}$$

describes the propagation of a front of a constant normal velocity, as noted before. In the general case, we can write

$$h_t = \nu\nabla^2 h - m\mathcal{H}(h_x) + \frac{\lambda}{2}(h_x)^2. \tag{15}$$

An equation of this type was also proposed by Yortsos [25] to describe the weakly nonlinear propagation of displacement fronts in porous media. Theoretical work performed by Thual, Frisch, and Henon [26] has shown that Eq. (15) admits a polar decomposition. This property is useful for analytical purposes and will be used later below to check the numerical results. The final step is to add noise to Eq. (15), leading to the HKPZ equation

$$h_t = \nu h_{xx} - m\mathcal{H}(h_x) + \frac{\lambda}{2}(h_x)^2 + \eta(x,t). \tag{16}$$

The random noise reflects heterogeneity and is typically an uncorrelated (in space and time) Gaussian with zero mean.

In the remainder of this section we will provide a derivation of the HKPZ equation for a model problem corresponding to reactive infiltration, for example, the acidization of a

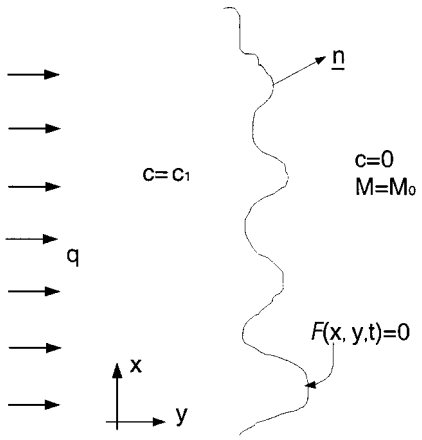

FIG. 1. Schematic of a reactive infiltration interface. Chemical injected upstream at concentration c_1 and rate q reacts infinitely fast at the reactive interface (front) with a mineral of initial concentration M_0. Both chemical and mineral are consumed completely at the interface. As a result of the reaction, the permeability changes in the two regions. The normal vector at the interface is indicated.

porous rock. To derive Eq. (15) we will apply first a linear and then a weakly nonlinear stability analysis.

A specific example from reactive infiltration

Consider the injection into a porous medium of a chemical at concentration c_1 and constant rate q. The chemical does not affect the fluid viscosity but it reacts with a mineral at the pore surface, of initial concentration M_0, and results in a change of the permeability of the porous medium, so that a permeability contrast $\kappa \equiv K_1/K_0$ develops. We assume that as a result of the reaction the mineral and the injected chemical are completely consumed. In this notation, subscripts 0 and 1 refer to the initial and injected states, respectively. We further assume that the reaction kinetics are fast, so that the reaction occurs over a surface (front). This requires large Damkholer numbers (see [27] for more details). Under this assumption, the reacting surface separates a downstream region, where the chemical concentration is identically zero and the mineral is at concentration M_0, from an upstream region, where the chemical concentration is variable due to diffusion and advection, while the mineral concentration is identically zero (see schematic in Fig. 1). One example for this problem could be the oxidation of minerals like pyrite or uraninite (UO_2). Although such a reaction usually leads to the formation of secondary mineral products, the oxygen is consumed at a redox front as the mineral dissolves. Other examples, for instance involving the dissolution of quartz, can be readily formulated as well. For the reaction we will take the simple scheme

$$\{\text{chemical}\} + \theta\{\text{mineral}\} \rightarrow \{\text{products}\}, \tag{17}$$

where θ is the stoichiometric coefficient of the reaction. In dimensionless notation (subscript D), the problem is described as follows.

Define the reacting front by the equation $\mathcal{F}(x_D, y_D, t_D) = 0$. Downstream of the front, $\mathcal{F} > 0$, we have

$$c_D = 0, \quad M_D = 1, \quad K_D = 1, \quad \mathbf{u}_D = -\boldsymbol{\nabla} p_D, \tag{18}$$

where the characteristic variables for the chemical concentration, the mineral concentration, the permeability, the velocity, and the pressure were taken as c_1, M_0, K_0, q, and $\mu(1+A)\mathcal{D}/K_0$, respectively. Here, μ is the fluid viscosity, $\mathcal{D}$ is the diffusion-dispersion coefficient, and A is a dimensionless constant expressing the capacity of the reactive process,

$$A = \frac{\phi \theta c_1}{M_0}, \tag{19}$$

where ϕ is upstream porosity. Implicit in the above is the use of the characteristic length $l = (1+A)\mathcal{D}/q$ and the use of Darcy's law for fluid flow in the porous medium. Upstream of the front, $\mathcal{F} < 0$, we have

$$M_D = 0, \quad K_D = \kappa, \quad \mathbf{u}_D = -\kappa \boldsymbol{\nabla} p_D \tag{20}$$

and

$$\frac{\partial c_D}{\partial t_D} + \mathbf{u}_D \cdot \boldsymbol{\nabla}_{c_D} = \frac{1}{(1+A)} \nabla^2 c_D, \tag{21}$$

where time was made dimensionless by $\phi l/q$. In either region, the continuity equation applies, namely,

$$\boldsymbol{\nabla} \cdot \mathbf{u}_D = 0, \tag{22}$$

where it was assumed that the mineral capacity is sufficiently large. The problem is completed by interface conditions. Across the front, the concentration of the chemical is continuous,

$$c_D = 0 \quad \text{at } \mathcal{F} = 0, \tag{23}$$

but the mineral concentration undergoes a jump from 0 to 1. In addition, conservation of mass leads to the following condition for the normal component of the front velocity:

$$v_{Dn} = -\frac{A}{(1+A)} \frac{\partial c_D}{\partial n} \tag{24}$$

where n denotes the direction of the unit normal $\mathbf{n}$ at the front (see Fig. 1).

We will consider, in sequence, the existence of a planar traveling wave under steady-state conditions, its linear stability, and its weakly nonlinear stability. For simplicity, and to be consistent with the rest of the text, the analysis is restricted to a 2D geometry.

The base state

The base state, denoted by an overbar, is a planar front traveling at the dimensionless velocity $\overline{v_D}$. In the limit of fast kinetics, the base-state concentration $\overline{c_D}$ is given by

$$\overline{c_D} = \begin{cases} 1 - \exp(\xi), & \xi < 0 \\ 0, & \xi > 0, \end{cases} \tag{25}$$

where we introduced the moving coordinate $\xi = y_D - \overline{v}_D t_D$. The base-state velocity $\overline{v}_D$ is found using Eq. (24),

$$\overline{v}_D = \frac{A}{(1+A)} < 1. \tag{26}$$

For the stability analysis, it is convenient to introduce a coordinate system moving with the front,

$$\rho = \xi - F(\tau, \xi), \quad \zeta = x_D, \quad \tau = t_D, \tag{27}$$

where F is the front perturbation relative to the moving coordinate [compare also with Eqs. (4) and (5)], based on which Eq. (21) becomes

$$\frac{\partial c_D}{\partial \tau} + (u_{D\rho} - \overline{v}_D - F_\tau - u_{D\zeta} F_\zeta) \frac{\partial c_D}{\partial \rho} + u_{D\zeta} \frac{\partial c_D}{\partial \zeta} = \frac{1}{(1+A)} \left[\frac{\partial^2 c_D}{\partial \rho^2} + \frac{\partial^2 c_D}{\partial \zeta^2} - F_{\zeta\zeta} \frac{\partial c_D}{\partial \rho} - 2F_\zeta \frac{\partial^2 c_D}{\partial_\rho \partial \zeta} + F_\zeta^2 \frac{\partial^2 c_D}{\partial \rho^2} \right]. \tag{28}$$

Darcy's law reads as

$$u_{D_\rho} = -\kappa \frac{\partial p_D}{\partial \rho}, \quad u_{D\zeta} = -\kappa \left[\frac{\partial \rho_D}{\partial \zeta} - F_\zeta \frac{\partial p_D}{\partial \rho} \right] \tag{29}$$

in the upstream region, and as in Eq. (29) but with 1 replacing κ in the downstream region. The continuity equation becomes

$$\frac{\partial u_{D\rho}}{\partial \rho} + \frac{\partial u_{D\zeta}}{\partial \zeta} - F_\zeta \frac{\partial u_{D\zeta}}{\partial \rho} = 0 \tag{30}$$

and the interface condition reads

$$\overline{v}_D + F_\tau = -\frac{A}{(1+A)} \left[\frac{\partial c_D}{\partial \rho} (1 + F_\zeta^2) - F_\zeta \frac{\partial c_D}{\partial \zeta} \right] \quad \text{at } \rho = 0. \tag{31}$$

Subscripts τ and ζ denote differentiation with respect to these variables.

Linear stability analysis

Consider next the linear stability analysis of the above system. We will take the general expansion

$$\psi_D = \overline{\psi}_D(\rho) + \Psi' \approx \overline{\psi}_D(\rho) + \epsilon \Psi(\rho) \exp(\omega \tau + ik\zeta). \tag{32}$$

Here Ψ' is the perturbation of the variable ψ, which in the linear stability limit is expressed in terms of normal modes, with ω being the rate of growth of a disturbance with wave number k, and i is the imaginary variable. Here, we have assumed that k is positive. More strictly speaking, one should use $|k|$ instead. Analogously, we will take $F \sim \exp(\omega\tau + ik\zeta)$. Substitution in the governing equations and linearization gives after considerable manipulations the eigenvalue condition for the determination of ω. Details are omitted and can be found in [27]. We obtain

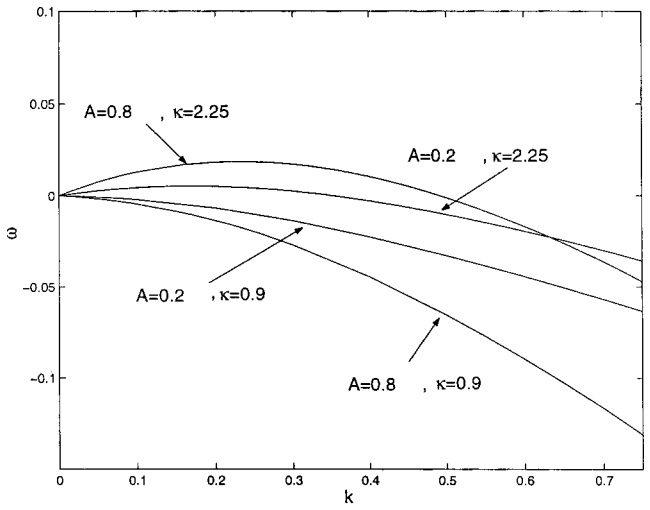

FIG. 2. The eigenvalue ω plotted as a function of the wave number k for different values of the permeability contrast κ. Long-wave instability is predicted for $\kappa > 1$, the process being stabilized at smaller wavelengths due to diffusion. Unconditional stability exists for $\kappa < 1$. Parameter A affects the numerical values of ω but does not change the qualitative nature of the instability.

$$\begin{aligned} &[A + A\sqrt{1 + 4(\omega^* + k^2)}][(\kappa+1)(k-\omega^*) \\ &\quad + k(\kappa-1)(A+1)] \\ &\quad = 2(A-\omega^*)(k-\omega^*)(\kappa+1) \\ &\quad + 2A(A+1)k(k+1)(\kappa-1), \end{aligned} \tag{33}$$

where we defined for simplicity $\omega^* = \omega(1+A)$. A plot of the admissible solution of Eq. (33) for ω as a function of k and for different values of κ is given in Fig. 2. As expected, the problem is unstable in a region of large wavelengths (small wave numbers) if $\kappa > 1$, and stable otherwise. The instability is driven by the change in permeability, which focuses flow toward the fingers and accentuates small disturbances. It is mitigated at smaller wavelengths by the diffusion of the chemical, which in this case acts to stabilize the system. We must note that Eq. (33) also accepts the trivial solution $\omega^* = 1$, which is not admissible, however, as the derivation was based on the assumption $\omega^* \neq 1$ (see [27]).

For the particular application in this paper, we must consider the roots of $\omega = 0$, which in addition to the trivial solution $k = 0$ can be readily shown to occur at the value k_c, where

$$k_c = \frac{(\kappa-1)[\kappa + 1 + (\kappa-1)(1+A)](1+A)}{(\kappa+1)[\kappa + 1 + 2(\kappa-1)(1+A)]}. \tag{34}$$

As expected, k_c vanishes as $\kappa \to 1$. Then an asymptotic expansion of Eq. (33) in this limit shows [27] that

$$\omega=\frac{A}{(A+1)}\frac{(\kappa-1)}{(\kappa+1)}k-\frac{2A\kappa[\kappa+1+A(\kappa-1)]}{(1+A)^2(\kappa+1)^2}k^2+\cdots. \tag{35}$$

Thus in the region of the onset of instability we have $k\sim\kappa-1$ and $\omega\sim(\kappa-1)^2$. It follows that if we consider long times and large wavelengths in this limit, the problem will become quasi-one-dimensional, as in [13]. This particular scaling will be considered in the nonlinear analysis to follow. Before we proceed, we also note that at this limit we have the scaling [27]

$$C'\sim C(\rho)\sim O((\kappa-1)^2),\quad U'_\rho\sim U_\rho(\rho)\sim O((\kappa-1)^2),$$

$$U_\zeta=-F_\zeta \tag{36}$$

for the leading-order expansion of the perturbations of the concentration and of the components of the two velocities.

Weakly nonlinear stability analysis

Consider, now, a weakly nonlinear analysis near the long-wave limit, which from Eq. (35) is meaningful when $\kappa\sim1$. We remark that a weakly nonlinear analysis of a similar problem was done in [28], but in a different context. In that analysis, the width of the system was finite, the marginal state such that the cutoff wavelength $\sim1/k_c$ is precisely equal to the width, and the system was weakly perturbed to an unstable state, ultimately leading to a Landau equation. An analogous approach for two-phase flow in porous media was done earlier in [29].

To proceed with our analysis we take again the expansion

$$c_D=\overline{c}_D(\rho)+C',\quad \mathbf{u}_D=\overline{\mathbf{u}}_D+\mathbf{U}'=\mathbf{i}_y+\mathbf{U}',$$

$$p_D=\overline{p}_D(\rho)+P' \tag{37}$$

where $\mathbf{i}_y$ is the unit vector in the main flow direction, and recognize that the perturbations have the order indicated in Eq. (36) in this limit. The equation for the perturbation in concentration reads

$$\frac{\partial C'}{\partial\tau}+(1-\overline{v}_D-F_\tau-U'_\rho-U'_\zeta F_\zeta)\frac{\partial C'}{\partial\rho}-(F_\tau-U'_\rho-U'_\zeta F_\zeta)\frac{\partial\overline{c}}{\partial\rho}+u'_\zeta\frac{\partial C'}{\partial\zeta}$$
$$=\frac{1}{(1+A)}\left[\frac{\partial^2C'}{\partial\rho^2}(1+F_\zeta^2)+F_\zeta^2\frac{\partial^2\overline{c}}{\partial\rho^2}+\frac{\partial^2C'}{\partial\zeta^2}-F_{\zeta\zeta}\frac{\partial\overline{c}}{\partial\rho}-2F_\zeta\frac{\partial^2C'}{\partial\rho\partial\zeta}\right]. \tag{38}$$

In the large-time [of $O(\kappa-1)^{-2}$)] and large-wavelength [of $O(\kappa-1)^{-1}$)] limits, recognizing the scaling (36) and assuming that $F=O(1)$, the disturbance of the concentration satisfies the following equation to order $(\kappa-1)^2$:

$$\frac{1}{(1+A)}\frac{\partial^2C'}{\partial\rho^2}-\frac{1}{(1+A)}\frac{\partial C'}{\partial\rho}=\left[U'_\rho-F_\tau-F_\zeta^2+\frac{F_{\zeta\zeta}}{1+A}\right]\frac{\partial\overline{c}}{\partial\rho}-\frac{F_\zeta^2}{1+A}\frac{\partial^2\overline{c}}{\partial\rho^2}. \tag{39}$$

Subsequent integration of Eq. (39) gives

$$\frac{1}{(1+A)}\frac{\partial C'}{\partial\rho}-\frac{1}{(1+A)}C'=-\int_0^\rho\exp(\rho)\left[U'_\rho-F_\tau-F_\zeta^2-\frac{F_\zeta^2}{1+A}+\frac{F_{\zeta\zeta}}{1+A}\right]d\rho+\frac{1}{(1+A)}\frac{\partial C'}{\partial\rho}\bigg|_0, \tag{40}$$

where we used the continuity condition $C'(\rho=0)=0$. The last term in the right-hand side of the above can be calculated using the interface condition (31). We find

$$\frac{1}{(1+A)}\frac{\partial C'}{\partial\rho}\bigg|_0=\frac{F_\zeta^2}{1+A}-\frac{F_\tau}{A}. \tag{41}$$

Then, evaluating Eq. (40) at $\rho=-\infty$ and requesting that the disturbance and its derivative vanish upstream, we obtain the following equation for F:

$$\frac{(A+1)}{A}F_\tau+F_\zeta^2-\frac{1}{(1+A)}F_{\zeta\zeta}+\int_0^{-\infty}\exp(\rho)U'_\rho d\rho=0. \tag{42}$$

The final step is to evaluate the disturbance for the velocity U'_ρ and insert it in Eq. (42). For this, we need to find the solution for the pressure disturbance in the limit taken, $\kappa\to1$. The latter can be shown [27] to be equal to

$$P'=\begin{cases}-\dfrac{F}{\kappa}+\Pi(\rho,\zeta,\tau), & \rho<0\\ -F+\Pi(\rho,\zeta,\tau), & \rho>0\end{cases}, \tag{43}$$

where Π satisfies the Laplace equation in the respective regions, along with continuity of pressure and mass at the front, $\rho=0$. By taking a Fourier transform on the variable ζ, we obtain the solution

$$\hat{\Pi}(\rho,k,\tau)=-\frac{(\kappa-1)}{\kappa(\kappa+1)}\hat{F}\exp(|k|\rho),\quad \rho<0, \tag{44}$$

which may then be used for the evaluation of $\hat{U}'_\rho=-\kappa\partial\hat{\Pi}/\partial\rho$. After some calculations we find

$$T_{\text{Fourier}}\left\{\int_0^{-\infty}\exp(\rho)U'_\rho d\rho\right\}=-\frac{(\kappa-1)}{(\kappa+1)}\frac{|k|\hat{F}}{(|k|+1)}, \tag{45}$$

which, in the limit of small k, can be inverted to

$$\int_0^{-\infty} \exp(\rho) U'_\rho d\rho = \frac{(\kappa-1)}{(\kappa+1)} \mathcal{H}(F_\zeta). \tag{46}$$

Finally, substituting back in Eq. (42) we find the desired equation

$$F_\tau + \frac{A}{(A+1)} F_\zeta^2 + \frac{A}{(A+1)} \frac{(\kappa-1)}{(\kappa+1)} \mathcal{H}(F_\zeta) - \frac{A}{(A+1)^2} F_{\zeta\zeta} = 0, \tag{47}$$

which is the HKPZ equation in the absence of noise, Eq. (15), with $h=F$, $t=\tau$, $x=\zeta$, $\lambda=-A/2(A+1)$, $m=[A/(A+1)](\kappa-1)/(\kappa+1)$, and $\nu=A/(A+1)^2$.

In the sections to follow, we will consider the general properties of the HKPZ equation. It must be recalled, however, that its validity for a physical process, e.g., of the reactive infiltration type, is subject to the restrictions of large wavelengths near the onset of instability (namely, when the destabilizing contrast is weak, $\kappa-1 \ll 1$, or small $m>0$). In the more general case of strong instability, the HKPZ equation does not generally apply and cannot capture Laplacian growth, which must be modeled instead by processes of the diffusion-limited-aggregation (DLA) type (e.g., see [15] and related references). In a sense, in the destabilizing case the HKPZ equation corresponds to the weak-instability limit, with DLA being its strong-instability counterpart.

Before closing this section, we must note that a similar analysis also applies for the diffusion-reaction system studied in [8]. In that application, there is no bulk flow; the chemical diffuses in the bulk and precipitates (or leads to a dissolution of the solid) at the reacting interface. In the schematic of Fig. 1 only the upstream region needs to be considered for this process. A first-order reaction is assumed to occur at the interface with kinetic constant $\mathcal{K}$ (units of velocity). The interface moves in the negative direction in the case of precipitation, and in the positive direction in the case of dissolution. One can then show by a linear stability analysis that the case of precipitation is long-wave unstable for the growing surface, the slope in the ω-k curve at the origin vanishing as the base-state velocity of the interface equals the kinetic velocity $\mathcal{K}$. The analysis is very similar to that for directional solidification [23,24]. Now, interface instability is driven by the nonlocal transport due to bulk diffusion. The process is stabilized by lateral diffusion along the interface, an interface condition for which can be postulated by partitioning the incoming flux partly to the interface growth along the normal [as in Eq. (31)] and partly to interfacial diffusion along the interface. For an equation of the KPZ type to result, the latter must be taken proportional to the curvature. For lack of space, this analysis will not be detailed here. If one proceeds along lines similar to the above, however, an equation similar to Eq. (15) is then derived. Thus, the process studied in [8] appears to fall in the HKPZ class also (in fact, in its unstable version, $m>0$).

In the remaining of this paper we will consider the solution of Eq. (16) and its linear counterpart in one space dimension. For this, we will first present the numerical scheme and then compare results against analytical solutions in the absence of noise. Then, the linearized HKPZ equation will be solved analytically. Finally, the full HKPZ equation will be solved numerically.

III. NUMERICAL SCHEME

Equation (16) was discretized numerically using standard methods. For spatial derivatives we used forward-backward finite differences of lattice constant Δx. The Hilbert transform was evaluated using a fast Fourier transform algorithm. The equation was marched in time using an Euler scheme with time increments Δt. Periodic boundary conditions were used for its solution. If grid points are labeled by integer n, the discretized version of Eq. (16) reads

$$h_n(t+\Delta t) = h_n(t) + \frac{\Delta t}{\Delta x^2}\{\nu[h_{n+1}(t) - 2h_n(t) + h_{n-1}(t)] + \tfrac{1}{8}\lambda[h_{n+1}(t) - h_{n-1}(t)]^2\} + m\Delta t I_n(t) + \Sigma\sqrt{12\Delta t} R_n(t), \tag{48}$$

where $I_n(t)$ is the discretized Hilbert transform calculated using a fast Fourier transform routine and we defined $\Sigma^2 = 2D/\Delta x$ (recall that D is related to the noise amplitude). The random numbers R_n are taken from a uniform distribution between $-\frac{1}{2}$ and $\frac{1}{2}$. The prefactor $\Sigma\sqrt{12\Delta t}$ guarantees that the noise has the same second moment as the Gaussian noise integrated over the time interval Δt [30]. In our simulations we have typically taken $\Delta x = 1$, $\nu = 0.5$, $\Sigma = 0.1$, and $\Delta t = 0.05$, while we varied λ and m. In all simulations, the initial condition is a flat interface, $h=0$ at $t=0$.

The accuracy of the numerical scheme was tested by comparing the numerical results against the analytical solution of a related equation in the absence of noise, namely, the extended Burgers equation [31]

$$v_t - 2vv_x + m\mathcal{H}v_x = v_{xx}, \tag{49}$$

which, as noted before, admits a polar decomposition [26]. This equation describes the evolution of the slope of the interface of Eq. (16), $v=h_x$, in the absence of noise and where $\nu=1$ and $\lambda=2$. For the periodic case of interest here, analytical results are possible for the one-''lump'' solution

$$v = n\{\cot[n(x+a)] + \cot[n(x+a^*)]\}, \tag{50}$$

where $2n$ is the wave number, the pole is described by the time-dependent complex variable $a=\phi+i\psi$ with $\psi>0$, and a^* denotes the complex conjugate. Substitution of Eq. (50) in Eq. (49) shows that ϕ is a constant, which we can take as $\phi(0)=0$, without loss in generality. We find

$$v = \frac{2n\sin(2nx)}{\cosh[2n\psi(t)] - \cos(2nx)}, \tag{51}$$

where $\psi(t)$ solves the equation

$$\psi'(t) = \frac{2n\sinh(4n\psi)}{\cosh(4n\psi) - 1} - m \tag{52}$$

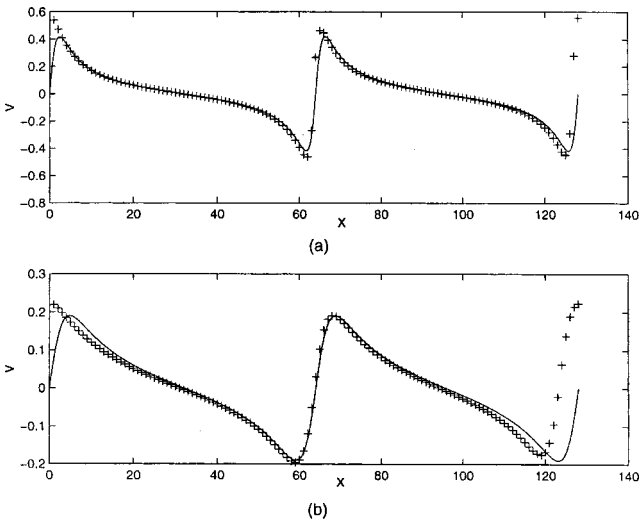

FIG. 3. Comparison of the analytical solution of the extended Burgers equation, denoted with a solid line, and the numerical solution, denoted with crosses, for two different times (a) $t=3.57$, (b) 51. The latter time corresponds effectively to a steady-state solution. Here $L=128$, $n=\pi/64$, and $m=0.2$.

and has the implicit solution

$$\frac{1}{(1+\gamma)}\ln\left|\frac{\exp(4n\psi)+(1+\gamma)/(1-\gamma)}{\exp[4n\psi(0)]+(1+\gamma)/(1-\gamma)}\right| - \left(\frac{1-\gamma}{1+\gamma}\right)2n[\psi-\psi(0)]=4n^2(1-\gamma)t, \tag{53}$$

where $\gamma\equiv m/2n$. For v to reach a nontrivial steady state requires $\gamma>1$ (i.e., $m>2n$) which, in this case ($\nu=1$), is identical to the condition for the existence of an unstable mode in the linear problem [dispersion relation (10)].

Analytical and numerical results are shown in Fig. 3 for the cases $\psi(0)=1$, $m=0.2$, and $n=2\pi/L$, where $L=128$ is the lattice size. Comparison is shown for two different times. The agreement between the solutions is very good, except near the end points of the simulation interval, where there is a small discrepancy that increases somewhat at larger times. Figure 3 implies the existence of a ''wrinkled'' front, the slope of the front increasing rapidly at the ends of the interval. This was noted in the simulations reported in [14,31,32]. The results of Fig. 3(b) essentially correspond to an asymptotic steady state, which, as expected from the theory, is reached in this case of $\gamma>1$. Here, the nonlinearity acts to stabilize the fastest growing mode. By contrast, if $\gamma<1$, the slope of the front eventually vanishes, all modes being stable. Excellent agreement between theory and numerical simulations was found for that case as well. Good agreement between theory and simulations was also found in testing more complex profiles that included more poles. From these examples it was concluded that the computational scheme would lead to accurate solutions of the HKPZ equation.

IV. THE LINEARIZED HKPZ EQUATION

Insight into the behavior of the HKPZ equation can be obtained by considering its linearized version

$$h_t=\nu h_{xx}-m\mathcal{H}(h_x)+\eta(x,t). \tag{54}$$

For its analysis, we follow previous work on the KPZ equation by Nattermann and Tang [33]. Consider a process with periodic boundary conditions, initiated at $t=0$ [and in which case $\eta(x,t)=0$ for $t<0$]. By applying a double Fourier transform in space and time, defined as

$$\hat{h}(k,\omega)=\int_{-\infty}^{\infty}\int_{-\infty}^{\infty}e^{-i(kx-\omega t)}h(x,t)dx\,dt, \tag{55}$$

Eq. (54) becomes

$$\hat{h}(k,\omega)=\frac{1}{(\nu k^2-m|k|)-i\omega}\,\hat{\eta}(k,\omega). \tag{56}$$

Equivalently, given that $\eta=0$ for $t<0$, we may take a Laplace transform in time. Proceeding as in [33] and noting that

$$\langle\hat{\eta}(k,\omega)\,\hat{\eta}(k',\omega')\rangle=2D(2\pi)\,\delta(k+k')\int_0^{\infty}e^{i(\omega+\omega')\tau}d\tau, \tag{57}$$

we find using Eq. (56) the result

$$\langle\hat{h}(k,t)\hat{h}(k',t)\rangle=\frac{2\pi D}{(\nu k^2-m|k|)}[1-e^{-2(\nu k^2-m|k|)t}] \times\delta(k+k'), \tag{58}$$

based on which we can calculate the mean-square width of the interface over the lattice,

$$w^2(L,t)=\langle[h(x,t)-\langle h(x,t)\rangle]^2\rangle =\frac{1}{4\pi^2}\int_{2\pi/L}^{\pi/\Delta x}\int_{2\pi/L}^{\pi/\Delta x}\langle\hat{h}(k,t)\hat{h}(k',t)\rangle dk\,dk'. \tag{59}$$

Note that the lower and upper limits of the integrals are $2\pi/L$ and $\pi/\Delta x$, respectively. Substitution of Eq. (58) and carrying out one integration yields

$$w^2(L,t)=\frac{1}{\pi}\int_{2\pi/L}^{\pi/\Delta x}\frac{D}{(\nu k^2-m|k|)}[1-e^{-2(\nu k^2-m|k|)t}]dk, \tag{60}$$

which can be further rearranged to read

$$w^2(L,t)=\frac{DL}{\pi\nu}\int_{2\pi}^{N\pi}\frac{1}{(z^2+cz)}[1-e^{-2b(z^2+cz)}]dz. \tag{61}$$

Here, we introduced the notation $N=L/\Delta x$, $z=kL$, $c=-mL/\nu=-k_cL$, and the dimensionless time $b=t\nu/L^2$. The effect of the nonlocal transport enters through parameter c, which is also proportional to the lattice size L. Note that the denominator in Eq. (61) is singular when $c<0$ (which cor-

responds to the destabilizing case); however, the singularity is removable. Equation (61) can be expressed in a compact form as

$$w^2(L,t)=\frac{DL}{\pi\nu}f(b;c,N), \tag{62}$$

where

$$f(b;c,N)=\int_{2\pi}^{\pi N}\frac{1}{z^2+cz}[1-e^{-2b(z^2+cz)}]dz. \tag{63}$$

We note that the existence of two dimensionless variables c and b, containing different t and L dependences, breaks the similarity scaling $t\nu/L^2$ applicable in the EW equation (where $c=0$); thus one expects a different scaling behavior.

In the following, we will consider the behavior of $f(b;c,N)$ in the two asymptotic limits of large and small times, respectively, for two different cases, a stabilizing case $c>-2\pi$, and a destabilizing case $c<-2\pi$ [and where we took into account the dispersion relation (10)]. For each case, we will consider the two different limits of large and small times.

A. The stabilizing case $c>-2\pi$

In the stabilizing case, and at large times ($b\gg 1$), the function $f(b;c;N)$ approaches the limit

$$f(b;c,N)\approx\frac{1}{c}\int_{2\pi}^{\pi N}\left(\frac{1}{z}-\frac{1}{z+c}\right)dz. \tag{64}$$

Due to the condition $c>-2\pi$, the above integral converges. Then, substitution in Eq. (62) gives the large-time result

$$w^2(L,t)\to w_\infty^2(L)=-\frac{D}{\pi m}\ln\left(\frac{1-mL/2\pi\nu}{1-m\Delta x/\pi\nu}\right). \tag{65}$$

Thus, in the stabilizing case the mean-square width saturates to a value which, for sufficiently large L, has a logarithmic dependence on L. This is to be contrasted with the power-law scaling $w^2\sim L$ that applies in the 1D EW equation. The latter scaling can also be derived from Eq. (65) in the limit $m\to 0$. The saturation width decreases with increasing $|m|$, reflecting the more compact nature of the front at increasing stabilization. The analytical results were confirmed using numerical simulations. Figure 4 shows a plot of $w_\infty^2(L)$ versus $\ln[(1-mL/2\pi\nu)/(1-m\Delta x/\pi\nu)]$, obtained numerically, for $m=-0.5$, $\nu=0.5$, and various lattice sizes up to $L=512$. In the simulations, the width was averaged over 100 realizations. The theoretical calculations predict a straight line with a slope equal to $-D/\pi m=0.0032$. The figure shows very good agreement between theory and simulations.

In the opposite limit of small times ($b\ll 1$), the integral in Eq. (63) can be manipulated to read as

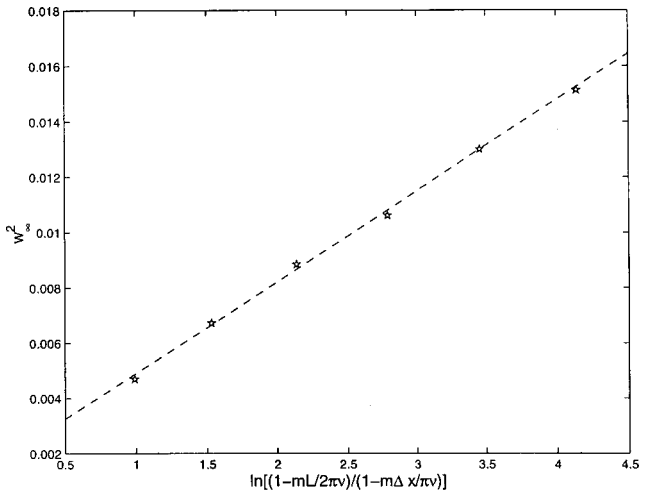

FIG. 4. Dependence of the saturation width on the lattice size for the linearized HKPZ equation in the stabilizing case and for large times. The numerical results are denoted by stars and correspond to $L=16,32,64,128,256,512$, respectively. Here, $m=-0.5$, and $\nu=0.5$. The width in the vertical axis is the ensemble average over 100 realizations. The dashed line corresponds to the analytically calculated slope $-D/\pi m=0.0032$.

$$f(b;c,N)=A(b;c,N)-\frac{1}{c}\ln\left(\frac{2\pi}{2\pi+c}\right)\times[1-e^{-2b(4\pi^2+2\pi c)}]-\frac{2b}{c}I, \tag{66}$$

where we introduced the function

$$A(b;c,N)=\frac{1}{c}\ln\left(\frac{\pi N}{\pi N+c}\right)-\frac{1}{c}\ln\left(\frac{\pi N}{\pi N+c}\right)e^{-2b(\pi^2N^2+c\pi N)}\approx-\frac{1}{\pi N}+O(e^{-2b\pi^2N^2}) \tag{67}$$

and the integral

$$I=\int_{2\pi}^{\pi N}\ln\left(\frac{z}{z+c}\right)(2z+c)e^{-2b(z^2+cz)}dz. \tag{68}$$

Note that the right-hand side of Eq. (66) is well defined in the limit $c\to-2\pi$, which is the point of transition from the stabilizing to the destabilizing case. This also suggests that the early-time scaling applies equally well to the destabilizing case. For sufficiently large discretization, $b\gg N^{-2}$, the parameter A tends to $-1/\pi N$, as in the EW equation, and where we implicitly assumed that $|m|\Delta x\ll\nu$. Thus, the first term in Eq. (66) (and the expansion for w^2) is infinitesimally small at large N. The contribution from the second term in Eq. (66) is $O(b)$; hence the leading-order term arises only from the integral I. For sufficiently large N, this becomes

$$I\approx\frac{2b}{c}\int_{2\pi}^{\infty}\ln\left(\frac{z}{z+c}\right)(2z+c)e^{-2b(z^2+cz)}dz, \tag{69}$$

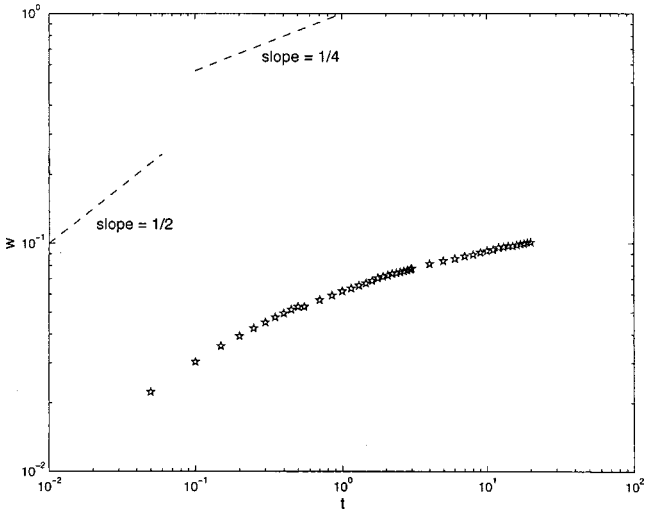

FIG. 5. Dependence of the ensemble-averaged width on time for the linearized HKPZ equation for the stabilizing case and at early times. The numerical results are denoted by stars. Here $L=256$, $m=-0.5$, and $\nu=0.5$. The dotted lines indicate the theoretically calculated slopes. The width is averaged over 100 realizations.

the asymptotic behavior of which at small b can be evaluated. After several manipulations, we obtain the result

$$I=\sqrt{2\pi b}+2b\int_{4\pi^2+2\pi c}^{\infty}\left(\ln\left[1-\frac{2c}{c+\sqrt{c^2+4t}}\right]+\frac{c}{\sqrt{t}}\right)dt + \cdots . \tag{70}$$

Thus, the leading-order term is $O(\sqrt{b})$, which when substituted in Eq. (62) gives the following small-time asymptotic result:

$$w^2(L,t)=-\frac{D\Delta x}{\pi^2\nu}+\frac{DL}{\pi\nu}[\sqrt{2\pi b}+O(b)+O(e^{-2b\pi^2N^2})]. \tag{71}$$

It follows that in the range $N^{-2}\ll b\ll 1$ the width of the front scales as a power law of time with exponent $\beta=\frac{1}{4}$. This scaling is identical to that of the EW equation, suggesting that in the small-time limit the nonlocal contribution does not enter to leading order. This regime is preceded by a linear scaling regime, the interval of which, $b\ll N^{-2}$, decreases with increasing N, and where the corresponding exponent is $\beta=\frac{1}{2}$. This interval and exponent also apply in the EW case.

The above results were confirmed using numerical simulations. Figure 5 shows a log-log plot of $w(L,t)$ vs time. The width is again averaged over 100 realizations of the noise, while the parameters in the simulations take the values $L=256$, $m=-0.5$, and $\nu=0.5$. Agreement between theory and simulation is good, the two different regimes at small times having the theoretical slopes of $\frac{1}{2}$ and $\frac{1}{4}$, respectively.

B. The destabilizing case $c<-2\pi$

In the destabilizing case, Eq. (10) shows that m must satisfy the constraint $m>2\pi\nu/L$, or, equivalently, $c<-2\pi$. Now, the denominator in Eq. (63) vanishes in the range of integration; however, the singularity is removable. The asymptotic properties of the solution in the two limits of large and small times, respectively, can be obtained by proceeding as follows.

To obtain the behavior of the solution at large times, we decompose the integral into two parts,

$$f(c;b;N)=\int_{2\pi}^{-c}\frac{1}{z^2+cz}[1-e^{-2b(z^2+cz)}]dz + \int_{-c}^{\pi N}\frac{1}{z^2+cz}[1-e^{-2b(z^2+cz)}]dz. \tag{72}$$

In the limit of large b, the second integral remains bounded, since $z^2+cz>0$, but the first integral does not. Thus, at large times, the dominant contribution arises from the first term only,

$$f(b;c,N)\sim\int_{2\pi}^{-c}\frac{1}{z^2+cz}[1-e^{-2b(z^2+cz)}]dz. \tag{73}$$

By further manipulating this integral using Watson's lemma [34], we get

$$f(b;c,N)\sim\frac{2\sqrt{2\pi}\exp(bc^2/2)}{c^2\sqrt{b}}, \tag{74}$$

and final substitution in Eq. (62) yields the asymptotic behavior of w at large times,

$$w\sim\left(\frac{2\pi\nu}{t}\right)^{1/4}\frac{\sqrt{2D}}{m}\exp\left(\frac{m^2t}{4\nu}\right). \tag{75}$$

As expected, the linearized equation results in exponential growth at large times. The unbounded growth reflects the absence of any stabilizing influence due to nonlinearity, which was demonstrated in the corresponding Eq. (49) (see also Olami *et al.* [17,32]). Equation (75) indicates that $\ln(w^2t^{1/2})$ is a linear function of time, with slope $m^2/2\nu$. Figure 6 shows the corresponding numerical results for the parameters $L=256$, $m=0.5$, and $\nu=0.5$. In agreement with the theory, the slope of the plot in Fig. 6 is very close to the theoretical $m^2/2\nu=0.25$. The scaling at early times for the destabilizing case is identical to that for the stabilizing, given that the nonlocal effect does not enter to leading order, hence a power-law scaling applies at early times.

The lack of simultaneous power-law scalings in the two limits (small and large times) is a consequence of the fact that the linear HKPZ equation does not admit a self-affine solution. Indeed, a scaling approach in which $x\to lx$, $h\to l^{\alpha}h$, and $t\to l^{z}t$ [2] cannot be simultaneously satisfied for the HKPZ equation due to the presence of the nonlocal term.

C. The correlation function

For completeness, we also present results for the correlation function (the semivariogram)

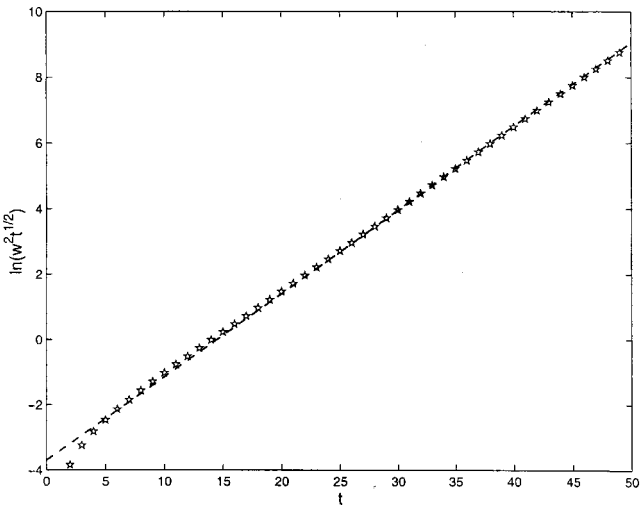

FIG. 6. Dependence of the ensemble-averaged width on time for the linearized HKPZ equation for the destabilizing case at large times. The numerical results are denoted by stars, where $L=256$, $m=0.5$, and $\nu=0.5$. The width is averaged over 100 realizations. The dashed line is the analytical calculation with slope $m^2/2\nu=0.25$.

$$C(r,t)=\langle|h(r,t)-h(0,t)|^2\rangle \tag{76}$$

for the case of an infinitely large lattice. Working similarly and following closely Ref. [33], we find the result

$$C(r,t)=\frac{2Dr}{\pi\nu}\int_0^\infty \frac{1-\exp[-2x(y^2+\lambda y)]}{y^2+\lambda y}(1-\cos y)dy, \tag{77}$$

where we introduced the variables $\lambda=-mr/\nu$ and $x=\nu t/r^2$. The behavior of $C(r,t)$ in the various asymptotic limits follows closely that of w^2. For both stabilizing and destabilizing case, the expansion at small r is linear,

$$C(r,t)\sim\frac{Dr}{\pi\nu}. \tag{78}$$

The correlation function increases with r and saturates at large r to a value increasing with time,

$$C(r,t)\to\frac{2D\sqrt{t}}{\pi\sqrt{\nu}}\int_0^\infty\frac{1}{z^2+\rho z}[1-\exp(-2z^2-\rho z)]dz \tag{79}$$

and where we introduced the time variable $\rho=-m\sqrt{t/\nu}$. In the stabilizing case $\rho>0$ and $C(r,t)$ approaches a limiting value at large times. In the destabilizing case $\rho<0$ and the large-time limit can be manipulated in the same manner as above to lead to an exponentially growing function,

$$C(r,t)\sim\exp\left(\frac{\rho^2}{2}\right)=\exp\left(\frac{m^2t}{2\nu}\right). \tag{80}$$

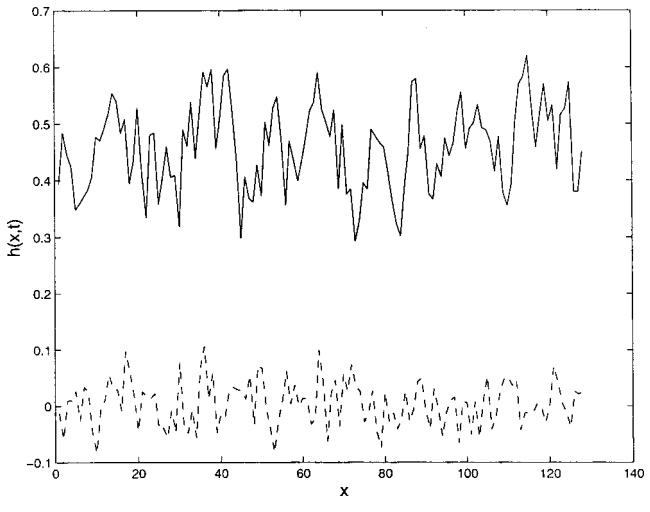

FIG. 7. Snapshots of the height $h(x,t)$ of the front of the HKPZ equation under stabilizing conditions for two different times $t=0.25$ (dotted line) and 50 (solid line). Here $L=128$, $m=-0.5$, $\nu=0.5$, and $\lambda=7$.

As before, the scaling behavior is affected by the presence of the nonlocal transport term m, which breaks the self-similarity and introduces additional dependences.

V. NUMERICAL SOLUTION OF THE HKPZ EQUATION

The preceding analysis suggests that the behavior of the HKPZ equation will also depend on whether the process is stabilizing or destabilizing. We used the numerical scheme described above to simulate the solution of the nonlinear equation in these two cases. Typically, the simulations were carried out starting from an initially flat interface. However, results were also obtained, particularly for the destabilizing case of the noiseless equation (15), starting from a random initial position.

Results corresponding to the stabilizing case are shown in Fig. 7. The figure shows snapshots of the front at early and late times. Both the front and its width increase with time and eventually approach a mean steady state, which fluctuates in both space and time. The presence of noise results in the constant fluctuation of the front around its mean value, in contrast to the flat front obtained asymptotically in the corresponding noiseless case, Eq. (51). In addition, and in contrast to the linearized case, the asymptotic mean position of the front is not zero, reflecting the effect of the nonlinear contribution. The variation with time of the width averaged over 100 realizations is shown in Fig. 8 for $L=128$, $m=-0.5$, and $\lambda=7$. For comparison purposes, also shown is the ensemble-averaged width corresponding to the KPZ equation with the same parameters. The scaling behavior of the width appears to be the same in the two equations at early times. However, as time proceeds the width of the HKPZ equation grows more slowly and saturates earlier and to smaller values, compared to those of the KPZ equation. This difference reflects the more compact front expected in the stabilizing HKPZ compared to the KPZ equation. We recall that in the KPZ equation the front has self-affine characteristics, with

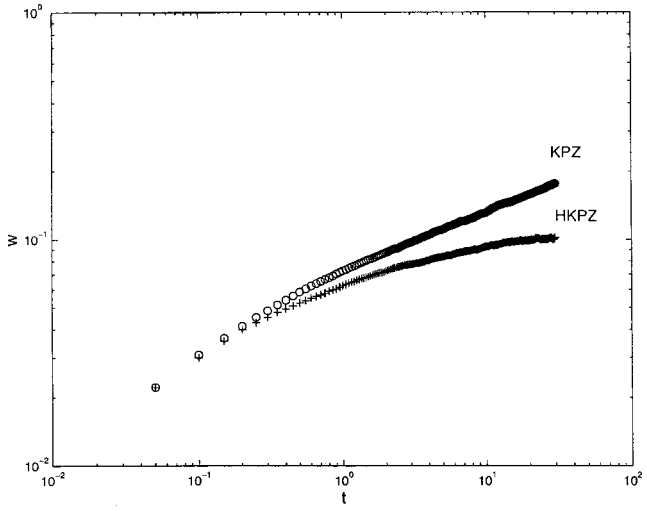

FIG. 8. Early-time behavior of the ensemble-averaged width for the KPZ (represented by circles) and HKPZ equations under stabilizing conditions (represented by crosses). Here $L=128$, $m=-0.5$, $\nu=0.5$, and $\lambda=7$.

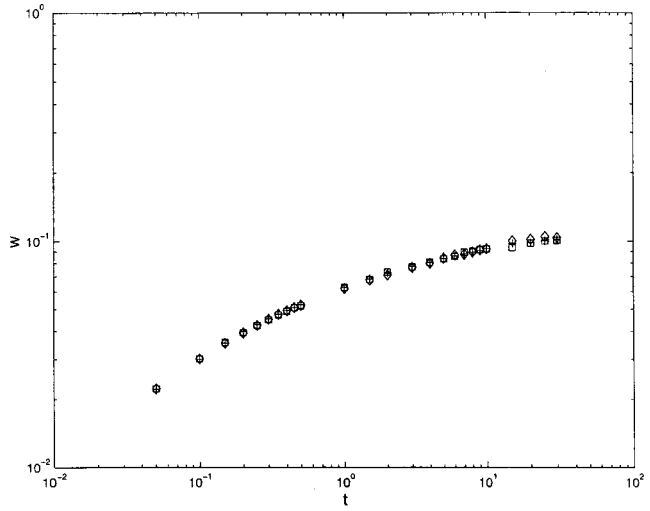

FIG. 9. Effect of λ on the dependence of the ensemble-averaged width of the HKPZ equation under stabilizing conditions, at early times and for three different values of λ [λ=1 (squares), 7 (crosses), 17.58 (diamonds)]. Here $L=128$, $m=-0.5$, and $\nu=0.5$.

the interface width satisfying the dynamic scaling

$$w(L,t)\equiv\langle[h(x,t)-\langle h(x,t)\rangle]^2\rangle^{1/2}\sim L^{\alpha}f(t/L^{\alpha/\beta}), \quad (81)$$

where $f(c)\sim c^{\beta}$ for $c\ll 1$, and $f(c)\to$const as $c\gg 1$. The growth exponent $\beta=\frac{1}{3}$ characterizes the time-dependent dynamics of the roughening process, while the roughness exponent $\alpha=0.5$ characterizes the roughness of the saturated interface [2]. Figure 8 suggests that the HKPZ equation also has an early-time power-law scaling similar to that of the KPZ, namely, with exponent $\beta=\frac{1}{3}$. The independence from the parameter m and the nonlocal character of the process, at early times, are consistent with the linearized HKPZ findings, where the early-time scaling is identical to that of the EW equation. The sensitivity of the early-time scaling to changes in various parameters was tested by varying L, m, and λ. Figure 9 shows that the behavior of the ensemble-averaged width is essentially unaffected by variations in λ. This was also the case for small values of λ. A similar effect was found for the KPZ equation as well. The effect of the nonlocal term is more important (Fig. 10) and affects the range of validity of the early-time power-law regime and the overall extent. As $|m|$ increases, the power-law scaling at early times lasts for a shorter period, and the width is smaller overall. As before, this reflects the stabilizing influence of nonlocal transport.

The dependence of the saturation width at large times on parameter m and the lattice size L is shown in Fig. 11. As before, larger values in the absolute magnitude of m lead to smaller asymptotic widths. The dependence on size is rather weak. If, in an attempt to satisfy Eq. (81), the curves were fitted with a power law, a small exponent α would result, estimated from the plot as $\alpha=0.19$. This exponent is considerably smaller than the corresponding roughness exponent of the KPZ equation, where $\alpha=0.5$. In analogy with the linearized HKPZ equation, we then elected to test the late-time results with a logarithmic function, of the form $w^2\sim\ln L$. The results are shown in Fig. 12 and demonstrate a good match for the three different values of m tested. The slope of the straight line is of the same order of magnitude as in the linearized case and decreases inversely proportionally to $|m|$, as $|m|$ increases. This is consistent with the findings from the linearized HKPZ equation. We are led to conjecture, therefore, that the scaling behavior of the HKPZ equation is not of the self-affine form (81), but that the early-time power-law scaling is followed at late times by a logarithmic dependence of the front width on the lattice size.

Subsequently, we studied the behavior of the HKPZ under destabilizing conditions, where $m>0$. As noted before, a rigorous analysis of the similar equation (9), which is the ex-

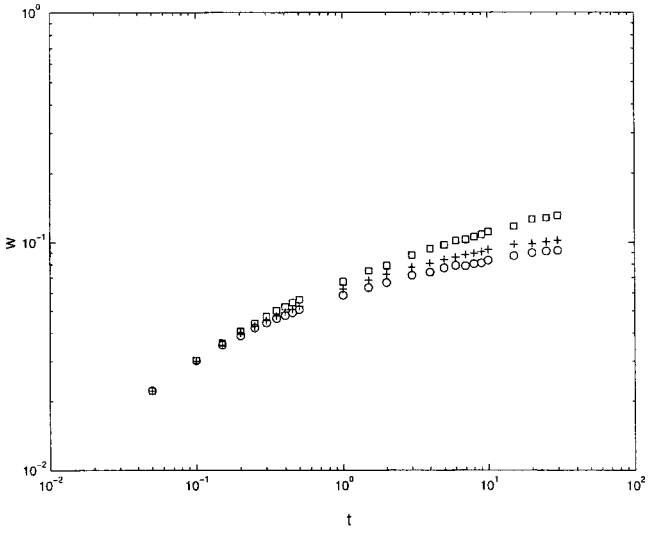

FIG. 10. Effect of m on the dependence of the ensemble-averaged width of the HKPZ equation under stabilizing conditions, at early times and for three different values of m [$m=-0.2$ (squares), -0.5 (crosses), -0.7 (circles)]. Here $L=128$, $\lambda=7$, and $\nu=0.5$.

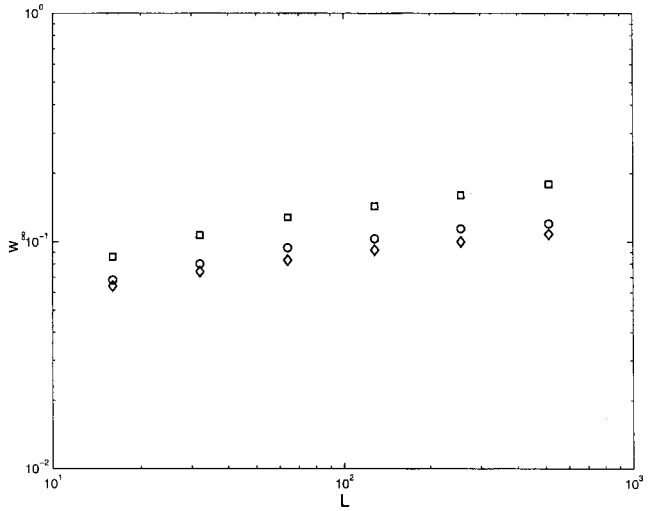

FIG. 11. Effect of m on the dependence of the ensemble-averaged width of the HKPZ equation under stabilizing conditions at late times [$m=-0.2$ (squares), -0.5 (circles), -0.7 (diamonds)]. Here $\lambda=7$ and $\nu=0.5$.

tended Burgers equation in the presence of noise, was undertaken by Olami *et al.* [17]. These authors examined a number of issues, including the evolution of the solution of Eq. (9) in the absence of noise but with noisy initial conditions, and the effect of noise. Although Eq. (9) is not the same as the HKPZ equation, we anticipate similar results. In the following we will discuss the solution of the destabilizing HKPZ equation in two cases, first in the absence of a noise forcing term but with noisy initial conditions, and second in the presence of a noise forcing term.

The results of a simulation of the noiseless HKPZ equation (15) in 1D, but with noisy initial conditions, are shown in Fig. 13 for different values of time. At early times, the front evolves in terms of well-defined fingers, the number of

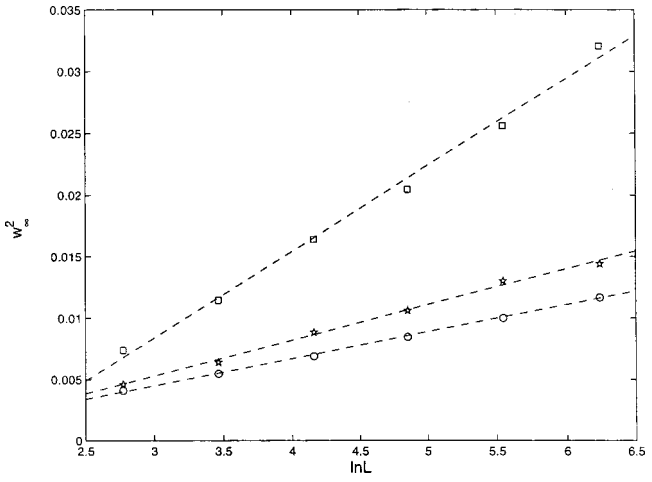

FIG. 12. Long-time behavior of the HKPZ equation under stabilizing conditions. The ensemble-averaged width shows logarithmic scaling with the lattice size L (where $L=16,32,64,128,256,512$). Numerical results are indicated by squares for $m=-0.2$, by stars for $m=-0.5$, and by circles for $m=-0.7$. Here $\nu=0.5$ and $\lambda=7$. The dotted lines indicate a least squares straight-line fit.

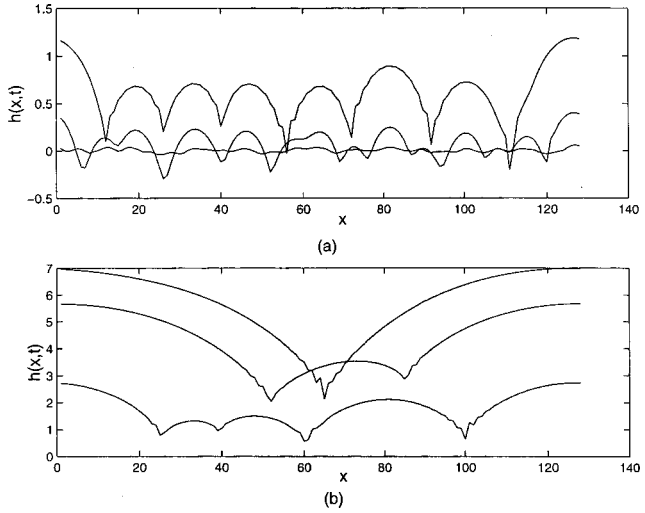

FIG. 13. Snapshots of the height of the interface of the noiseless HKPZ equation under destabilizing conditions starting from a noisy initial condition. In plot (a) the time is $t=5,25,50$ from bottom to the top. In plot (b) the time is $t=100,200,250$ from bottom to the top. Here $L=128$, $m=0.5$, $\nu=0.5$, and $\lambda=7$.

which decreases as time increases [Fig. 13(a)]. At later times the shape of the front changes to a few dominant fingers and the development of a ''giant'' cusp [Fig. 13(b)]. These features are very similar to those observed by Olami *et al.* [17], who explained the attraction to a giant cusp by using polar decomposition. We expect that similar arguments will hold here as well. The evolution of the width of the front as a function of time is plotted in Fig. 14. Following an initially slow variation, the width enters a regime that can be approximated as a power law $w\sim t^{\zeta_1}$ with an exponent estimated to be $\zeta_1=1.2$. This value is similar to that reported by Olami *et al.* [17] for the different equation they studied. Figure 14 also shows that the width stabilizes asymptotically to a value expected to be size dependent.

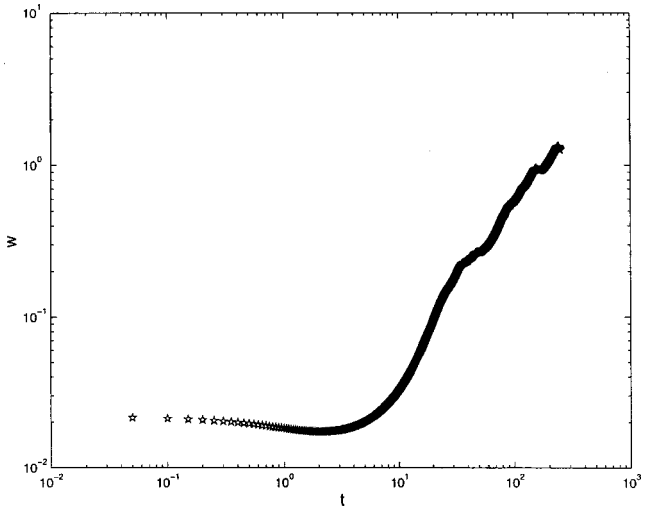

FIG. 14. Ensemble-averaged width for the noiseless HKPZ equation under destabilizing conditions starting from a noisy initial condition, corresponding to Fig. 13. Here $L=128$, $m=0.5$, $\nu=0.5$, and $\lambda=7$.

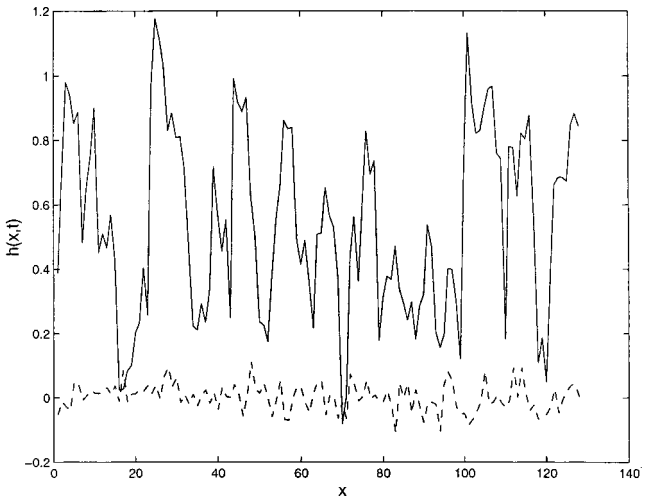

FIG. 15. Snapshots of the height $h(x,t)$ of the front of the HKPZ equation under destabilizing conditions starting with a flat initial condition. Dotted line, $t=0.25$; solid line, $t=10$. Here $L=128$, $m=0.5$, $\nu=0.5$, and $\lambda=7$.

Results for the simulation of the full HKPZ equation in the presence of noise and for the destabilizing case are shown in Fig. 15. Comparison with Fig. 13 shows a qualitatively different behavior. The number of fingers does not decrease significantly as time increases, while it does not appear that an attracting cusp actually exists. The additive noise present in the HKPZ equation continuously adds new poles, altering the dynamics of the noiseless equation (15). As explained in [17], the asymptotic state of the noiseless equation is nonlinearly unstable, thus leading to a qualitatively new regime. The behavior in Fig. 15 has features similar to those in regime II of Olami *et al.* [17], where noise is of sufficiently large amplitude. Figure 16 shows the variation of the ensemble-averaged width with time for this case. It indicates a continuous growth, with the late-time behavior resembling a power-law regime $w\sim t^{\zeta_2}$, with the exponent estimated at $\zeta_2\approx 1.1$.

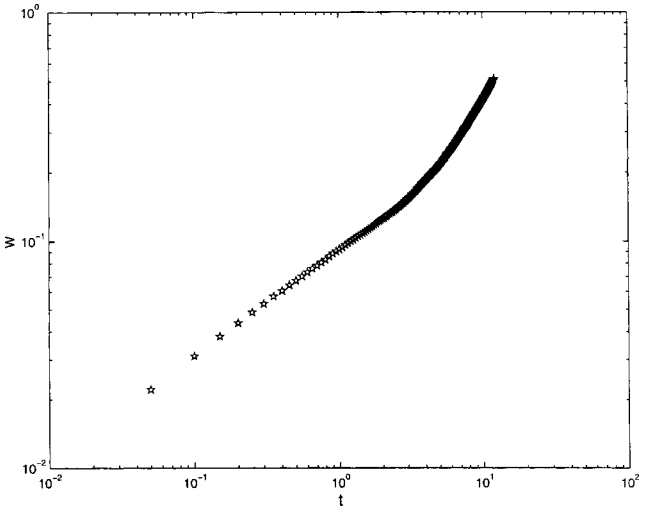

FIG. 16. The ensemble-averaged width of the HKPZ equation under destabilizing conditions as a function of time. Here $L=128$, $m=0.5$, $\nu=0.5$, and $\lambda=7$.

VI. CONCLUSIONS

In this paper, we derived an equation that extends the well-known KPZ equation in order to capture nonlocal transport effects, through a Hilbert transform term. This equation, termed the HKPZ equation, can be used to describe the long-wave dynamics, near the onset of the nonlocal transport and in the weakly nonlinear limit, of various physical processes, where the nonlocal transport is governed by the Laplace equation and the stabilizing term is a second-order diffusion process. The nonlocal term may lead to processes that can be linearly stable or unstable, depending on the parameter values. A specific example from reactive infiltration was studied and was shown to lead in the weakly nonlinear limit to the noiseless HKPZ equation. The solution of the HKPZ equation in one dimension was considered by developing an appropriate numerical scheme, the accuracy of which was shown by comparison with the extended Burgers equation in the absence of noise. An analytical solution to the latter is possible through a pole decomposition method.

Then, the linear version of the HKPZ equation was investigated. Asymptotics for small and large times were developed and the appropriate scaling behavior was obtained analytically in these limits. The early-time behavior was found to be independent of the nonlocal transport term, hence identical to that for the EW equation, for either the stabilizing or the destabilizing case. This behavior is a power law with exponent $\beta=\frac{1}{4}$. In the stabilizing case, the width saturates at large times to a value that has a logarithmic dependence on lattice size, reflecting the nonlocal character of the process. This is different from the EW equation, where a power-law regime applies. In the destabilizing case, the late-time behavior is exponential growth with a rate corresponding to the fastest growing mode of the linear dispersion relation, as expected.

Subsequently, the full HKPZ equation was solved numerically in one spatial dimension. For the stabilizing case, the dynamical exponent was found to be identical to that of the KPZ equation, hence to not be affected by the nonlocal term. On the other hand, the long-time behavior appears to obey a logarithmic scaling with respect to the lattice size. The large-time scaling is also sensitive to the nonlocal transport parameters. For the destabilizing case, we found results similar to Olami *et al.* [17]. The noiseless equation, but with noisy initial condition, showed attraction to a giant cusp. However, the solution of the HKPZ equation in the presence of noise showed continuous fluctuations, and the absence of a dominant giant cusp. The width at late times was found to obey a power-law growth.

These results should find direct applications to the dynamics of growing interfaces, where the flux to the interface is controlled by a nonlocal Laplacian transport. Such applications are many and cover a broad range of physical processes. For example, they may include the displacement of viscous fluids in porous media, convection-reaction in porous media with permeability changes, reaction-diffusion processes on pore surfaces with morphological changes, and flame propagation. We also believe that the process studied in [8] falls in the same class. The effect of the non-

local term becomes important at large times, the early-time behavior being controlled by the KPZ dynamics. In the stabilizing case ($m<0$), the width asymptotically stabilizes; however, the power-law prediction of the KPZ equation must now be replaced by a logarithmic dependence on the lattice size. This dependence breaks down the spatiotemporal self-affinity of the KPZ interfaces, and also leads to more compact fronts. The development of more compact fronts is a result of the stabilizing influence of nonlocal transport. Under such conditions, therefore, one should use caution before applying the scalings derived from the KPZ equation. In the destabilizing case, the evolution of interfaces at large times also shows behavior significantly different from that of the KPZ equation. Specifically, the front width does not saturate at large times but rather increases as a power law in time, reflecting the frontal instability. We must note that for a physical application, for example, in reactive infiltration, the validity of this scaling is subject to the restrictions of large wavelengths near the onset of instability (namely, when the destabilizing contrast is weak, $\kappa-1\ll 1$, or small, $m>0$). In the more general case of strong instability, the HKPZ equation does not apply and cannot capture Laplacian growth, which must be modeled instead by processes such as diffusion-limited aggregation (e.g., see [15] and related references). In a sense, in the destabilizing case the HKPZ equation corresponds to the weak-instability limit, with DLA being its strong-instability counterpart.

ACKNOWLEDGMENTS

This work was partly supported by Los Alamos National Laboratory (P. K.). The research of Y. C. Y. was supported by the Department of Energy through Contract No. DE-AC26-99BC15211. Both contributions are gratefully acknowledged.

[1] M. Kardar, G. Parisi, and Y. Zhang, Phys. Rev. Lett. **56**, 889 (1986).
[2] A. L. Barabasi and H. E. Stanley, *Fractal Concepts in Surface Growth* (Cambridge University Press, Cambridge, 1995).
[3] P. Meakin, P. Ramanlal, L. M. Sander, and R. C. Ball, Phys. Rev. A **34**, 5091 (1986).
[4] R. Jullien and R. Botet, Phys. Rev. Lett. **54**, 2055 (1985).
[5] R. Jullien and R. Botet, J. Phys. A **18**, 2279 (1985).
[6] A. R. Kerstein and W. T. Ashurst, Phys. Rev. Lett. **68**, 934 (1992).
[7] M. Kardar and Y. C. Zhang, Phys. Rev. Lett. **58**, 2087 (1987).
[8] E. Aharonov and D. H. Rothman, J. Geophys. Res. B **101**, 2973 (1996).
[9] *Reactive Transport in Porous Media*, Vol. 34 of *Reviews in Mineralogy*, edited by P. C. Lichtner, C. I. Steefel, and E. H. Oelkers (Mineralogical Society of America, Washington, DC, 1996).
[10] T. Dogu, Chem. Eng. J. **21**, 213 (1980).
[11] G. F. Froment, in *Catalyst Deactivation*, edited by B. Delmon and G. F. Froment (Elsevier, Amsterdam, 1980).
[12] G. M. Homsy, Annu. Rev. Fluid Mech. **19**, 271 (1987).
[13] G. I. Sivashinsky, Acta Astronaut. **4**, 1177 (1978).
[14] D. M. Michelson and G. I. Sivashinsky, Acta Astronaut. **4**, 1207 (1978).
[15] G. Daccord and R. Lenormand, Nature (London) **325**, 41 (1987).
[16] A. Erdelyi, F. Oberhettinger, and F. G. Tricomi, *Tables of Integral Transforms*, Bateman Manuscript Project (McGraw-Hill, New York, 1954).
[17] Z. Olami, B. Galanti, O. Kupervasser, and I. Procaccia, Phys. Rev. E **55**, 2649 (1997).
[18] S. F. Edwards and D. R. Wilkinson, Proc. R. Soc. London, Ser. A **381**, 17 (1982).
[19] P. G. Saffman and G. I. Taylor, Proc. R. Soc. London, Ser. A **245**, 312 (1958).
[20] Y. C. Yortsos and F. J. Hickernell, SIAM (Soc. Ind. Appl. Math.) J. Appl. Math. **49**, 730 (1989).
[21] E. J. Hinch and B. S. Bhatt, J. Fluid Mech. **212**, 279 (1990).
[22] J. D. Sherwood, Chem. Eng. Sci. **42**, 1823 (1987).
[23] J. S. Langer, Rev. Mod. Phys. **52**, 1 (1980).
[24] P. Pelce, *Dynamics of Curved Fronts* (Academic, Boston, 1988).
[25] Y. C. Yortsos, J. Phys.: Condens. Matter **2**, SA443 (1990).
[26] O. Thual, U. Frisch, and M. Henon, J. Phys. (France) **46**, 1485 (1985).
[27] P. Kechagia (unpublished).
[28] J. Chadam, P. Ortoleva, and A. Sen, SIAM (Soc. Ind. Appl. Math.) J. Appl. Math. **48**, 1362 (1988).
[29] E. D. Chikhliwala and Y. C. Yortsos, SPE Reservoir Eng. **1-2**, 1268 (1988).
[30] K. Moser, J. Kertesz, and D. Wolf, Physica A **178**, 215 (1991).
[31] H. V. McConnaughey, G. S. S. Ludford, and G. I. Sivashinsky, Combust. Sci. Technol. **33**, 113 (1983).
[32] O. Kupervasser, Z. Olami, and I. Procaccia, Phys. Rev. Lett. **76**, 146 (1996).
[33] T. Nattermann and L.-H. Tang, Phys. Rev. A **45**, 7156 (1992).
[34] G. F. Carrier, M. Krook, and C. Pearsosn, *Functions of a Complex Variable* (McGraw-Hill, New York, 1966).